Localization of Multiple DNA Sequences on Nanopatterns

M. Serdar Onses,[†] Piyush Pathak,[‡] Chi-Chun Liu,[†] Franco Cerrina,[‡] and Paul F. Nealey[†,*]

[†]Department of Chemical and Biological Engineering, University of Wisconsin—Madison, Wisconsin 53706, United States and [‡]Department of Electrical and Computer Engineering, University of Wisconsin—Madison, Wisconsin 53706, United States

ABSTRACT DNA oligonucleotides of different sequences were patterned at the nanoscale. Areas of positive charge were generated by exposure of insulating substrates, spin-on hydrogen silsesquioxane or vapor-deposited SiO_2 on Si, with ionizing radiation sources used in electron beam and extreme ultraviolet lithography. Au nanoparticles (NPs) with a diameter of 15 nm, carrying covalently bound negatively charged single-stranded DNA oligonucleotides, were site specifically immobilized directly on the exposed regions and presented oligonucleotides for subsequent hybridization. Repeated exposure and deposition of NPs allowed for patterning multiple DNA sequences. Patterns with dimensions as small as 15 nm were fabricated using electron beam lithography. The use of DNA-functionalized NPs rather than just DNA facilitates metrology in scanning electron microscopy and improves the hybridization efficiency of the oligonucleotides on the surface.

KEYWORDS: DNA · nanopatterning · lithography · nanoparticles · hybridization

Sequence-specific base pairing of DNA oligonucleotides anchored to a surface is central to fields such as gene analysis,[1] biosensors,[2] and assembly of other nanomaterials.[3,4] The ability to pattern DNA oligonucleotides of different sequences at the nanoscale with high resolution, minimum nonspecific binding to background, and high hybridization efficiency will enable advancements and new applications. One potential area of immediate impact is the use of DNA for nanoscale patterning and fabrication on surfaces. Self-assembly of DNA molecules into nanostructures is a highly promising approach to control the organization of materials on surfaces at the nanometer length scale. DNA nanostructures[5] may be created, for example, by programmed interactions of oligonucleotides through Watson—Crick base pairing. The recently developed technique of "scaffolded DNA origami"[6] enables the formation of arbitrary shaped DNA nanostructures. The sequence information encoded in DNA origami can later be used to direct the assembly of other functional materials such as nanoparticles,[7] proteins,[8] and carbon nanotubes,[9] all with a precision of ~6 nm. A key challenge to advance the capabilities of DNA origami for the fabrication of nanoscale devices is devising parallel methods for placing and registering the DNA nanostructures in desired locations at the surface. Placement of DNA origami from solutions onto specific positions on a substrate has been previously demonstrated by generating binding sites based on electrostatic interactions,[10,11] Au—thiol binding,[12] and sequence-specific base pairing.[13] A degree of orientation control of the origami with respect to the substrate has been demonstrated by matching the geometry[10] and spacing[12] of the binding sites with the shape of DNA origami and the length of the DNA nanotube, respectively. Sequence-specific base pairing of oligonucleotides carried by DNA origami with substrate-bound complementary strands has great potential for the site-specific placement of multiple structures with a high degree of orientation control provided that oligonucleotides of multiple sequences are patterned and registered at the nanoscale over wafer size areas.

Patterning DNA has been previously demonstrated at sub-100 nm dimensions using direct printing of oligonucleotides, dip-pen nanolithography, and electron beam lithography. Direct printing techniques[14—16] are promising with respect to high throughput and low cost; however, resolution and/or pattern fidelity and registration are poor compared to lithographic methods. On the other hand, dip-pen nanolithography[17] is a technique that provides both high resolution and sequence diversity at the nanoscale. Even though there has been significant progress[18] in the development of high-throughput and inexpensive scanning probe lithography techniques, localization of multiple DNA sequences at the nanometer length scale using the highly developed advanced lithography infrastructure of the microelectronics industry will be beneficial for many applications.

* Address correspondence to nealey@engr.wisc.edu.

Received for review June 9, 2011 and accepted September 7, 2011.

Published online September 07, 2011
10.1021/nn2021277

In techniques based on electron beam lithography, nanopatches of oligonucleotides were typically generated by creating specific regions that were available for the DNA immobilization chemistries. Au pads, for example, may be patterned in a SiO_2 background using a lift-off process followed by the immobilization of thiol-functionalized oligonucleotides, leading to specific attachment of DNA molecules to the pads.[4,19] In another example,[20] regions of SiO_2 were patterned at the nanoscale in an octadecyltrimethoxysilane background. Functionalization of the substrate with a two-step linker chemistry led to specific attachment of oligonucleotides to the SiO_2 patterns. Alternatively, oligonucleotides were directly synthesized/immobilized[21] on a nanopatterned negative tone photoresist on a silicon background by multistep functionalization of the substrate. Despite the different techniques developed, the ability to pattern DNA oligonucleotides using lithographic techniques simultaneously meeting sub-50 nm resolution, minimal nonspecific binding to background and high hybridization efficiency remains a challenge. Moreover, one common limitation of the techniques that employed electron beam lithography is that nanopatterns of only one sequence have been demonstrated. A partial solution to this problem is to control the hybridization events by electric fields:[19] electrodes bearing the same sequence of oligonucleotides can be selectively turned on and off to control the hybridization with the complementary oligonucleotides carrying different functional groups. The use of electric fields provides a promising means for dynamic assembly of DNA molecules; however, the challenge of nanoscale patterning of multiple sequences on the surface remains unsolved.

RESULTS AND DISCUSSION

In this study, we demonstrate site-specific immobilization of multiple DNA sequences on nanopatterns created by advanced lithographic tools. It is known that surface charging occurs following the electron beam exposure of an insulator.[22−24] Recently Chi *et al.*[25] have shown that the positive charge generated at the top surface of a SiO_2 insulating layer by the electron beam exposure can be used to immobilize negatively charged DNA molecules at the nanoscale. Here we demonstrate that through judicious choice of exposure conditions and substrates and by immobilizing oligonucleotides conjugated to Au nanoparticles (DNA-Au NPs) instead of just oligonucleotides, nanopatterns of DNA can be obtained using the positive charge generation on insulators by the electron beam exposure with sub-50 nm resolution, minimal nonspecific binding to background, and high hybridization efficiency. In this approach, DNA-Au NPs are directly immobilized on the electron beam exposed regions of the insulating layers, allowing a photoresist-free patterning and one-step DNA immobilization. Localization of multiple DNA sequences at the nanoscale is accomplished by repeating the exposure and immobilization for each sequence. Repeating the process for each sequence requires the patterning and the immobilization to be noninterfering; each step should be mild enough not to foul the other one. Previously reported techniques using electron beam lithography typically required harsh conditions for removing the photoresist such as treatment in an acidic or basic solution, which might damage the immobilized DNA molecules. On the other hand, multistep immobilization chemistries might cause side/exchange reactions with the previously patterned DNA molecules, leading to loss of sequence specificity. Therefore, other than simplicity, photoresist-free patterning and one-step DNA immobilization enable the generation of arrays of patterned DNA oligonucleotides of different sequences on the surface. We also show that this strategy for the immobilization of DNA molecules can be generalized to the other ionizing radiation sources such as those used in highly parallel extreme ultraviolet (EUV) lithography.

The process scheme for the localization of multiple DNA sequences on nanopatterns is shown in Figure 1. An insulating layer was deposited on a silicon wafer either by spin-coating a 40 nm thick film of hydrogen silsesquioxane (HSQ) or by plasma-enhanced chemical vapor deposition of a 100 nm thick SiO_2. Patterns of positive charge were then defined by electron beam or EUV lithography based on exposure of the insulating layer with the ionizing radiation sources. DNA-Au NPs having many DNA strands per particle were prepared by functionalization of 15 nm Au NPs with disulfide-modified oligonucleotides according to the previously published protocol.[26] DNA-Au NP conjugates (1 nM) in 0.3 M sodium chloride/10 mM sodium phosphate buffer were spotted onto the patterned region for 1 h, and substrates were then washed with 0.3 M sodium chloride and water and then dried with N_2. Negatively charged DNA-Au NPs selectively attached to the positively charged exposed regions with minimal nonspecific adsorption to nonexposed background regions. The exposure and immobilization were repeated with Au NPs carrying different DNA sequences, creating nanoscale patterned arrays of multiple DNA sequences.

Previously[25,27] it has been shown that oligonucleotides in a buffered solution bind specifically to the positively charged regions generated by electron beam exposure of an insulating substrate. Here we use Au NPs as carriers for oligonucleotides for three purposes: (i) Au NPs can be easily functionalized with oligonucleotides; (ii) the conjugation of negatively charged oligonucleotides on the Au NPs enables two critical functions: a fraction of oligonucleotides participates in the specific attachment of particles to the positively charged regions of the substrate and the

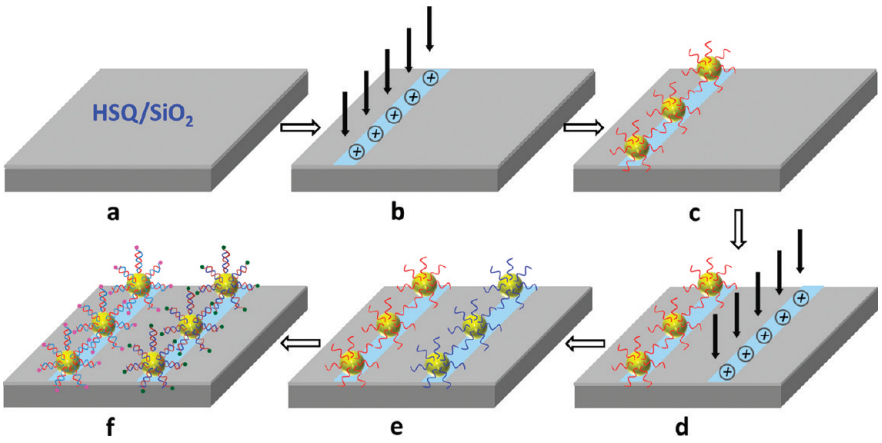

Figure 1. Process scheme for the localization of multiple DNA sequences on nanopatterns. (a) Spin-coated HSQ or vapor-deposited SiO_2 is used as an insulating layer on Si. (b) Nanopatterns of positive charge are generated by electron beam or EUV lithography based on exposure of an insulating layer to an ionizing radiation source. (c) Negatively charged DNA-Au NPs selectively bind to the positively charged patterns. (d) Exposure is repeated to generate a second set of positively charged patterns. (e) DNA-Au NPs with the second sequence are immobilized on the second set of patterns. (f) Specific hybridization from a mixture of fluorophore-labeled oligonucleotides (Cy3-Comp1, Cy5-Comp2) complementary to the sequences on the particles.

oligonucleotides on the Au NP that are not involved in attachment remain available for hybridization in high densities; (iii) Au NPs provide easy and quantitative characterization of the process at the nanoscale by direct imaging with a scanning electron microscope (SEM). We show that DNA-Au NPs can be specifically immobilized on patterned regions at a high density, and repeated exposure and deposition of DNA-Au NPs provide nanopatterns of multiple sequences on the surface. Hybridization of fluorophore-labeled complementary oligonucleotides leads to high-contrast fluorescence. These results suggest that this method can enhance the efforts using DNA in different applications including nanopatterning by providing a way to pattern DNA with specificity and size control at the nanoscale using the advanced lithography infrastructure.

Formation of positively charged patterned regions by electron beam lithography and the resulting attachment of DNA-Au NPs depended strongly on the electron beam energy (E_B) and the dose. In order to study the attachment behavior of DNA-Au NPs onto the exposed regions and to find exposure conditions for high attachment densities, $2 \times 2\ \mu m^2$ pads were patterned at an E_B of 1 and 20 keV on the same sample surface in a dose range of $50-4000\ \mu C/cm^2$, and DNA-Au NPs were immobilized onto the patterns. Samples were then imaged with SEM, as Au NPs provided high contrast. As can be seen in representative images given in Figure 2A, the density of attachment increased with increasing dose and decreasing E_B. In order to quantify the effect of exposure parameters, three spots for each dose and E_B were imaged with SEM at 50 000× magnification, and then, a representative, smaller area ($500 \times 500\ nm^2$) was chosen from each image and NPs were manually counted (see Supporting Information for the details of image analysis and additional SEM images). Figure 2B shows the average number of NPs per square micrometer with respect to dose for HSQ and SiO_2 at an E_B of 1 and 20 keV. The most critical parameter for the attachment density of DNA-Au NPs was the E_B: exposures performed at 1 keV resulted in higher densities of DNA-Au NP attachment than the exposures at 20 keV for the entire dose range studied. At low doses, up to 4 times more DNA-Au NP binding was observed at an E_B of 1 keV in comparison to an E_B of 20 keV. The attachment density of conjugates increased with the dose in the range of $0-500$ and $0-2000\ \mu C/cm^2$ at an E_B of 1 and 20 keV, respectively, and then reached a plateau. There was not any discernible difference in the density of attachment of DNA-Au NPs between HSQ and SiO_2 as a substrate.

Comparing the attachment behavior of DNA-Au NPs to the electron beam exposed insulating substrates with the previous study reveals some similarities and differences: Chi *et al.*[25] studied the effect of the E_B and the dose on the binding of λ-DNA to glass substrates that were exposed using electron beam lithography. Similar to our study, they observed more DNA binding following exposures at low $E_B = 5$ keV than at high $E_B = 30$ keV for the majority of the dose range. On the other hand, the dependence of the attachment density on electron beam dose differed between the two studies. For example, in the study by Chi *et al.*[25] the density of λ-DNA attachment was very low for exposures performed at doses $\leq 400\ \mu C/cm^2$ for both $E_B = 5$ keV and $E_B = 30$ keV. In our study, the density of DNA-Au NPs on the surface was significantly higher for exposures at 1 keV in comparison to 20 keV at doses $\leq 500\ \mu C/cm^2$. The differences in the attachment behavior of λ-DNA and DNA-Au NPs in the two studies may originate from experimental differences such as the size and type of DNA molecules and the method of DNA detection on

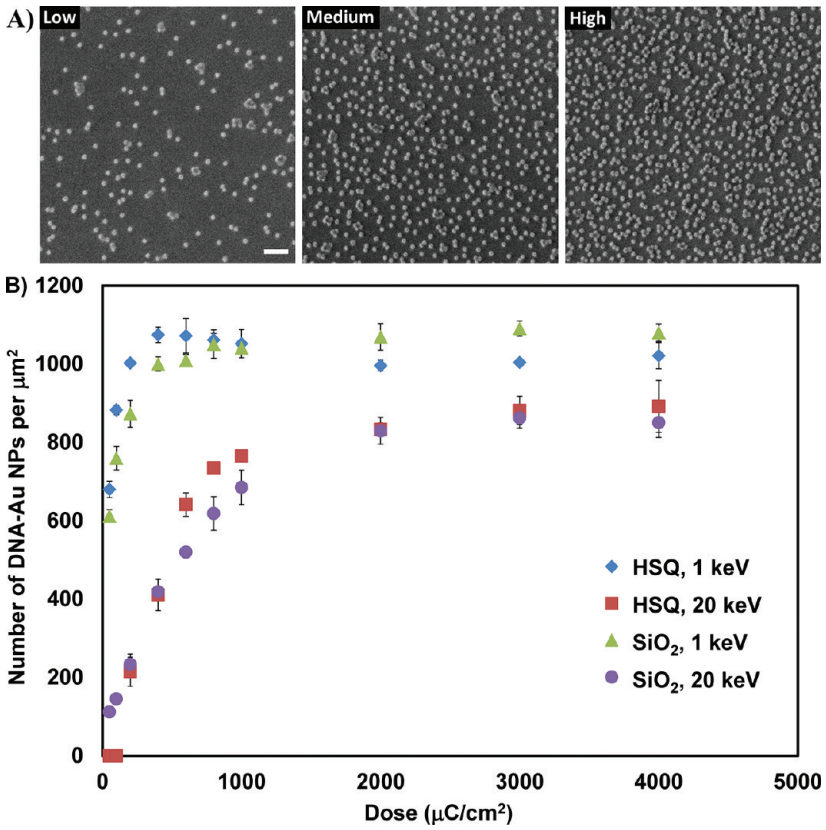

Figure 2. Effect of E_B and dose on the attachment density of DNA-Au NPs. (A) Representative SEM images on HSQ showing low (E_B = 20 keV, dose = 200 μC/cm^2), medium (E_B = 1 keV, dose = 50 μC/cm^2), and high (E_B = 1 keV, dose = 400 μC/cm^2) density of DNA-Au NPs on patterned features. Scale bar 100 nm. (B) Attachment density of DNA-Au NPs as a function of E_B, dose, and substrate. Each point in the plot is an average count obtained from three different spots.

the surface. λ-DNA, for example, is a large (48 502 base pairs) double-stranded DNA molecule with a radius of gyration of ~0.7 μm,[28] whereas DNA-Au NPs are assemblies of single-stranded oligonucleotides of 30−45 base pairs long on a 15 nm particle. Deriving quantitative attachment density from fluorescence imaging of immobilized λ-DNA molecules may also be leading to complications in comparison to the density of DNA-Au NPs on the surface simply obtained by the number of particles counted from SEM images.

We hypothesize that the attachment density of DNA-Au NPs correlates with the amount of positive charge formed during electron beam exposure. As can be seen in Figure 2B, an E_B of 1 keV resulted in higher densities of DNA-Au NP attachment than an E_B of 20 keV. This behavior supports the hypothesis, as it is in good agreement with the previous literature about the charging of insulators, that more electrons are emitted from the surface for the exposures performed at 1 keV than 20 keV.[22,23,29] Charging of insulators with electron beam exposure is typically described with secondary electron yield, which is the ratio of electrons emitted from the insulating layer to injected electrons.[22,29] With increasing E_B, secondary electron yield increases, reaches a maximum, and then starts to decrease. Secondary electron yield is greater than 1, and the net charge in the insulating layer is positive between two critical energies E_1 and E_2. At energies greater than E_2, secondary electron yield falls below 1 and decreases with increasing E_B.[22,23,29] Even if the net charge in the insulating layer is negative for the electron beam energies higher than E_2, a positive charge at the near surface is expected due to the local escape of secondary electrons.[30] Since E_1 is hundreds of eV[29] and E_2 is typically 1−3 keV for many insulators including SiO_2,[22] E_B of 1 keV used in this study is between E_1 and E_2, where secondary electron yield is greater than 1. On the other hand, 20 keV is much larger than E_2, in a regime (secondary electron yield < 1) where only a fraction of injected electrons are emitted from the surface. Therefore, more positive charge on the surface and more negatively charged DNA binding are expected at an E_B of 1 keV than 20 keV.

In order to gain insight into the charge formation upon exposure of the insulating layers used in this study, we used the molecular Monte Carlo simulation tool (MMC) developed by Pathak and Cerrina.[31] MMC simulates the exposure of a solid medium (*e.g.*, photoresist) with an energetic radiation source such as electron beam, extreme ultraviolet, and X-ray radiation, by modeling the physical processes involved in energetic particle−matter interaction. MMC generates detailed

information on the trajectory of electrons and their interaction with the medium. SiO_2 used in the experiments was modeled on the basis of atomic composition (SiO_2) and density (2.198 g/cm^3). Charge formation in HSQ cannot be accurately simulated, as the chemical composition and the density of HSQ change[32] during the electron beam exposure. Simulations were generated with 10 000 primary electrons in order to have statistically significant results. All ionizing events leading to positive charging through the insulating layer were mapped, and the number of ionizing events per primary electrons defined as ionizing yield was calculated for the conditions studied in the actual experiments. MMC predicted that ionizing yield for SiO_2 is about 3 times higher at an E_B of 1 keV than 20 keV (Table 1). This contrast in charging is consistent with the experimentally observed 2−4 times higher density of DNA-Au NP attachment for the exposures performed at 1 keV in comparison to 20 keV in a dose range ($\leq$1000 μC/cm^2) where there are no saturation effects (Figure 2B). At a dose of 400 μC/cm^2, for example, the attachment density of DNA-Au NPs to the patterned regions on SiO_2 is 2.4 (1000/419, Table 1) times higher at E_B = 1 keV than E_B = 20 keV. These results support the hypothesis that the attachment density of DNA-Au NPs correlates with the amount of positive charge formed during electron beam exposure.

Electron beam exposure of the insulating layers may result in alterations of the surface properties of the materials beyond the formation of positive charges. Both HSQ and SiO_2 are subject to structural/chemical transformations upon electron beam exposure. HSQ ($H_2Si_2O_3$) becomes rich in Si−O bonds[32] and resembles a SiO_2-like structure. During this transformation, the wetting behavior of HSQ also switches from hydrophobic to hydrophilic in the patterned regions.[33] The density and stoichiometry of SiO_2 can vary with the electron beam exposure,[34] and the presence of hydrocarbon vapors in the vacuum chamber can also lead to changes in surface chemistry due to deposition of carbonaceous materials.[35,36] This deposition process (taken to the extreme when used as a contamination resist) usually changes the wetting behavior of the patterned SiO_2 regions from hydrophilic to hydrophobic. Doses (10^5−10^6 μC/cm^2)[35] required for significant deposition are about 1000 times higher than the doses used in this study. Since the attachment densities (Figure 2B) of DNA-Au NPs are similar for a wide range of doses on HSQ and SiO_2 insulating layers, but the changes in surface chemistry and wetting properties of HSQ and SiO_2 with electron beam exposure are orthogonal, we believe that the dominant mechanism of particle binding is electrostatic interactions between the negatively charged DNA-Au NPs and the positively charged regions of the substrate.

Resolution of the patterns and nonspecific adsorption on the background are critical aspects of the process. Site-specific attachment of DNA-Au NPs onto electron beam patterned 100 nm wide lines on HSQ and SiO_2 can be clearly seen in SEM images given in Figure 3A and B, respectively. As with the density of attachment, HSQ and SiO_2 showed similar behavior in the generation of patterns and the site-specific attachment of DNA-Au NPs. In principle, resolution of the patterns is determined by the capabilities of the lithography system used, and it is possible to generate single particle (15 nm diameter) wide lines with the proper design of the size and dose of the patterns (Figure 3C, more SEM images of small line width patterns can be found in the Supporting Information). To the best of our knowledge, this line width is the highest resolution DNA pattern reported using lithographic processes. Another strength of the process relates to inherently low levels of nonspecific adsorption in the background regions (see Supporting Information for additional SEM images). Here a key point is the simplicity of the process, as there is no blanket chemical functionalization step involved; only the desired areas are altered to be attractive for DNA adsorption, so the rest of the surface keeps its original properties. It is known that SiO_2 is slightly negatively charged in neutral aqueous solutions[37] and has low levels of DNA adsorption in the absence of divalent ions.[10] On the other hand, the hydrophobicity of unexposed HSQ might be responsible for low levels of DNA adsorption in the background regions.

The functionality of immobilized DNA-Au NPs was verified by hybridization of fluorescently labeled complementary oligonucleotides. For this purpose, 100 nm wide lines of a single sequence (DNA-1, Table 2) were prepared following the process scheme given in Figure 1A−C. Surfaces were then treated with a prehybridization solution to condition the surface and to block patterned sites against any non-sequence-specific interactions during hybridization. A hybridization mixture containing complementary oligonucleotides labeled with Cy3 (Comp-DNA 1, Table 2) was then applied to the substrates for 2 h. Substrates were washed in buffers of decreasing salt concentration, dried, and then imaged with a fluorescence microscope. The fluorescence image presented in Figure 3D shows that immobilized DNA-Au NPs were functional and oligonucleotides could be specifically hybridized

TABLE 1. Ionizing Yield and Attachment Density of DNA-Au NPs at Different Electron Beam Energies for SiO_2[a]

electron beam energy	ionizing yield	number of particles per μm^2 (dose = 400 μC/cm^2)
1 keV	14.5	1000
20 keV	5.0	419

[a] The ionizing yields were obtained from molecular Monte Carlo simulation. The attachment densities of particles were taken from the experimental results given in Figure 2B.

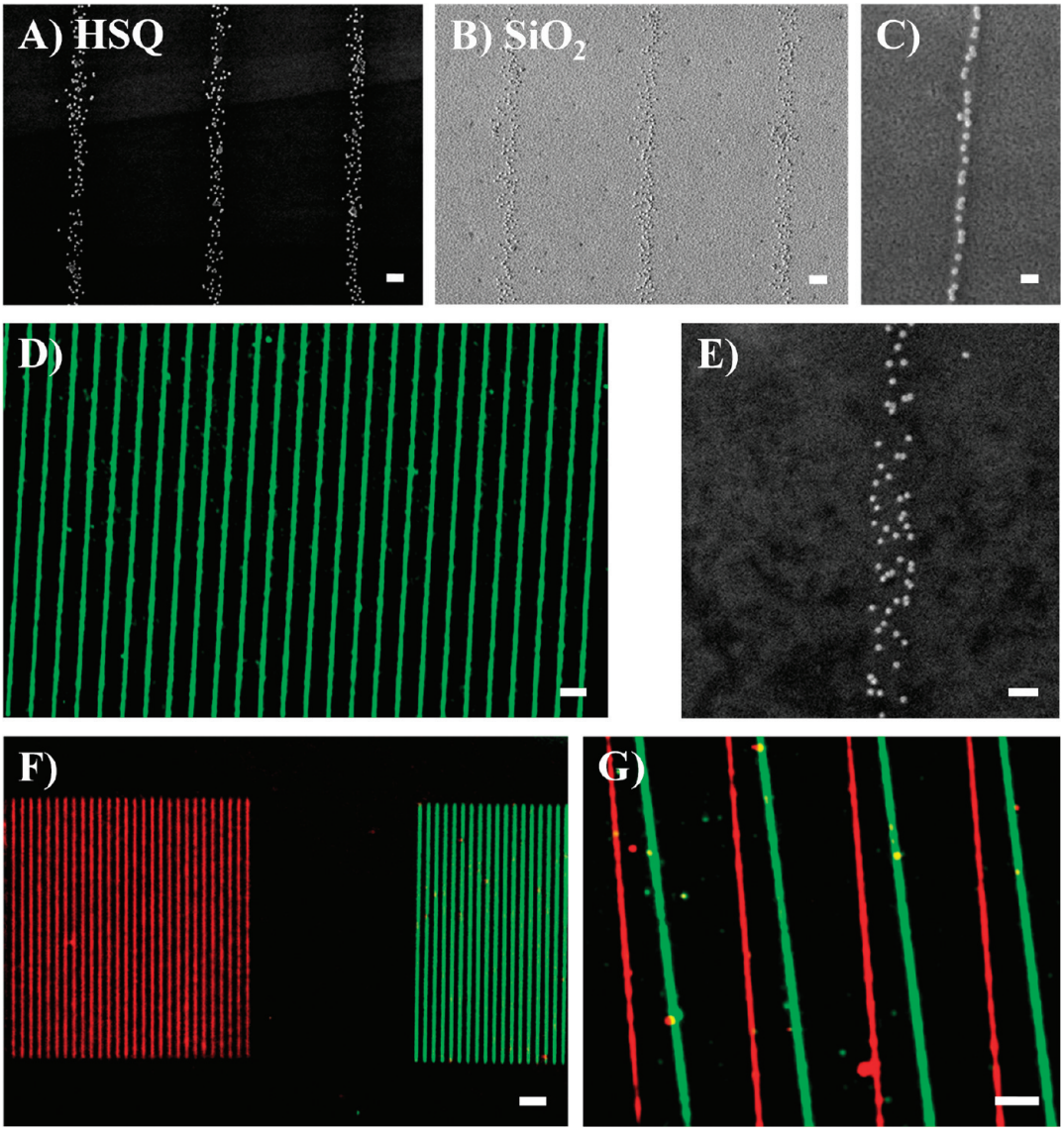

Figure 3. Site-specific placement of DNA-Au NPs on nanopatterns generated on HSQ and SiO_2 and hybridization with complementary oligonucleotides. (A, B) SEM images of electron beam patterned features following the attachment of DNA-Au NPs (scale bar 100 nm). (C) SEM image of single-particle 15 nm wide lines on HSQ (scale bar 50 nm). (D) Fluorescence image following the hybridization of Cy3-labeled complementary oligonucleotides onto DNA-Au NPs on HSQ following the placement of a single sequence (scale bar 10 μm). (E) SEM image following the hybridization (scale bar 100 nm). (F, G) Fluorescence images following the hybridization onto double-patterned substrates: For each image two different sequences of DNA-Au NPs were sequentially patterned, and then a mixture of fluorophore-labeled (Cy3, green; Cy5, red) complementary oligonucleotides was hybridized. DNA-Au NPs carrying a sequence complementary to the Cy3-labeled oligonucleotides were patterned first. (F) Two sets of 100 nm lines with 10 μm spacing patterned on SiO_2 each having a different sequence (scale bar 20 μm). (G) Closer alignment: Alternating 100 nm wide lines of two sequences on HSQ (scale bar 5 μm).

onto 100 nm wide lines. The absence of fluorescence signal in the case of hybridization with a noncomplementary sequence (NON-Comp DNA, Table 2) verified the sequence-specific interactions. As with the density of attachment, hybridization gave similar results on HSQ and SiO_2. A representative SEM image (Figure 3E) following the hybridization shows the presence of NPs on the patterned features, verifying the survival of DNA-Au NP attachment to the hybridization and washing process.

The use of NPs provides an easy way for quantitative analysis of oligonucleotide density on the surface, as the number of oligonucleotides on a single Au NP can be either measured[38] or calculated:[26] assuming roughly 50 oligonucleotides per particle based on the previous study[38] for a surface density of ~1000 NPs per μm^2 leads to the oligonucleotide density of $\sim 5 \times 10^{12}/cm^2$. If we assume that only the oligonucleotides on the top half of the particles are available for hybridization as the rest of them will face the surface, then the effective density of oligonucleotides is estimated to be $\sim 2.5 \times 10^{12}/cm^2$. This density is comparable with the previously reported values ranging from 1×10^{12} to $9 \times 10^{12}/cm^2$ obtained by immobilization of end-functional DNA on glass and gold using linker chemistries.[39]

TABLE 2. Sequences of Oligonucleotides Used in the Study

name	sequence
DNA-1	5′-TCT CAT TAT AGC TGC ATG ATA CAC TTC ACC $(T)_{15}$-3′-S-S
DNA-2	5′-GTT AAT TCT CCC GTC TAA TGT TTT TTT TTT TTT TT-3′-S-S
Comp-DNA-1	5′-GGT GAA GTG TAT CAT GCA GCT ATA ATG AGATTT TT-3′-Cy3
Comp-DNA-2	5′-CAT TAG ACG GGA GAA TTA ACT TTT T-3′-Cy5
NON-Comp DNA	5′-GGG CGG CGA CCT TTT T-3′-Cy3

One advantage of using DNA-Au NPs compared to oligonucleotides is the improved availability of the recognition sites for the hybridization. The orientation of the oligonucleotides is critical for the all DNA immobilization schemes, as it determines the accessibility to the target oligonucleotides.[40] Therefore improving hybridization efficiencies necessitates the use of end-functionalized oligonucleotides attached to a surface directly or through use of a linker molecule. Consideration of low hybridization efficiencies has been a limitation in the use of electrostatic binding in the microarray applications,[41,42] as the whole oligonucleotide is bound to the surface and not fully available for the hybridization. In our system, a portion of oligonucleotides on the NPs is used for the attachment and the remaining oligonucleotides are available for the hybridization as they are end-bound to the particle surface through the thiol bond. In order to compare the hybridization efficiencies with and without NPs as carriers, immobilization was performed with 10 μM oligonucleotides and 1 nM DNA-Au NPs in 0.3 M sodium chloride/10 mM sodium phosphate buffer on a HSQ-coated substrate. The concentration of oligonucleotides was chosen relatively high for two reasons: (i) to account for the presence of many oligonucleotides per particle; (ii) to be in the concentration range (1 μM to 1 mM) used in previous studies for the immobilization of end-functionalized oligonucleotides on homogeneous[40,43] and patterned[19,20] substrates. Following the hybridization with Cy3-labeled complementary oligonucleotides, fluorescence microscope images of 1 μm wide lines were taken and intensity profiles were measured. Due to the complications of comparing fluorescence intensities from different substrates, fluorescence contrast defined as the ratio of fluorescence intensity from patterns to fluorescence intensity from nonpatterned (background) regions was used as a measure of the process. Using DNA-Au NPs provided about 4 times (Figure 4) more fluorescence contrast than using just oligonucleotides. This result suggests that the efficiency of hybridization is higher with the conjugates in comparison to oligonucleotides, assuming the nonspecific binding to the background is at similar levels in both cases as all the conditions (buffer, sequence, substrate, *etc.*) except the concentration of DNA molecules are the same.

We demonstrated the ability to localize multiple DNA sequences on the nanopatterns by repeating

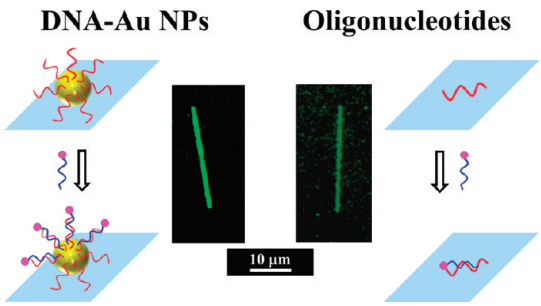

Figure 4. Fluorescence images following the hybridization of Cy3-labeled complementary oligonucleotides onto patterned DNA-Au NPs and oligonucleotides on HSQ. Concentrations of DNA-Au NPs and oligonucleotides were 1 nM and 10 μM, respectively. Ratio of fluorescence signal from lines to background is 8.1 for DNA-Au NPs and 2.2 for oligonucleotides.

the exposure and immobilization with two different DNA-Au NPs (DNA-1 and DNA-2, Table 2). Hybridization with complementary strands bearing fluorophores (Comp-DNA-1-Cy3 and Comp-DNA-2-Cy5, Table 2) was used to verify the patterning process. Fluorescence images of the same region were taken with two different excitation/emission filters, and images were merged using ImageJ software. As can be clearly seen in Figure 3F and G, Cy3- and Cy5-labeled target oligonucleotides were specifically directed to the first and second patterned areas, verifying the double patterning. In Figure 3F, the two sets of 100 nm lines with 10 μm spacing patterned 50 μm away on SiO_2 are shown. An example of closer alignment is given in Figure 3G with the patterning of 100 nm wide lines alternating at 5 μm on HSQ, demonstrating the finer placement of lines. Alignment of multiple sequences with sub-10 nm accuracy can be possible with the use of state-of-the-art tools and techniques that have been developed for the microelectronics industry.[44]

Besides presenting a solution to the challenge of nanoscale patterning of multiple sequences on surfaces, repeated immobilization of different sequences of DNA-Au NPs on nanopatterns gives some insights into the strength of interaction between the conjugates and the substrate. The strong sequence-specific fluorescence from the 100 nm wide lines (Cy3-green in Figure 3F and G) that are generated in the first patterning step points to the strength of the binding between DNA-Au NPs and the surface of the substrate, as these conjugates experienced a series of washing (in different buffers) and annealing (during prehybridization and hybridization). The strength of interaction is such that patterned substrates could be washed with water following immobilization of DNA-Au NPs and dried with N_2. This strength stands in contrast to desorption[45] of DNA nanostructures following a rinse with water from patterned oxide surfaces where the binding is based on electrostatic interactions mediated by Mg^{2+}. It is also important to note that immobilization of second DNA-Au NPs and hybridization of Cy5-labeled

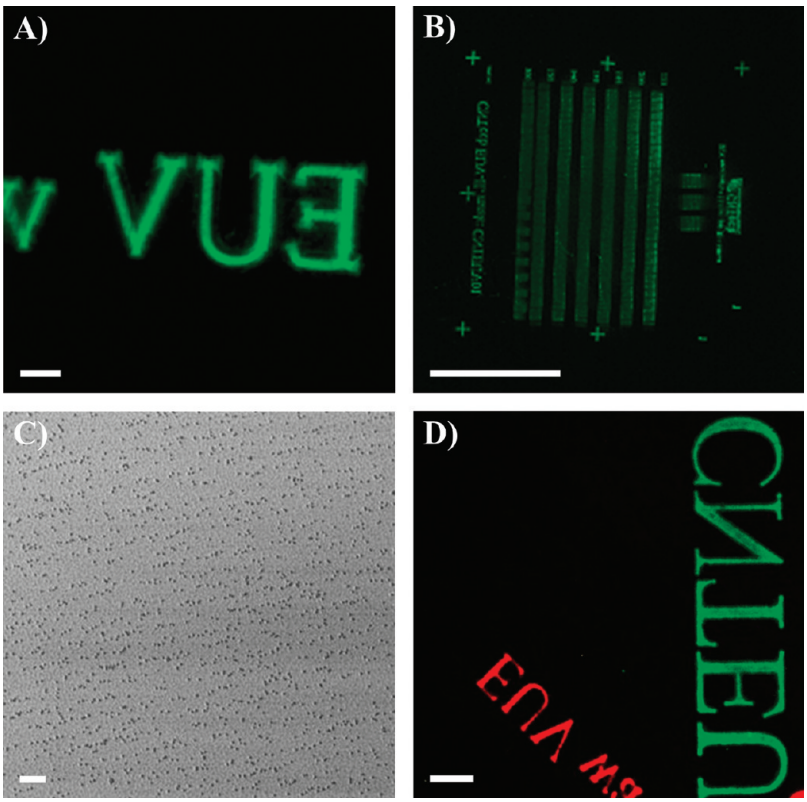

Figure 5. A different radiation source: EUV. (A) Fluorescence microscope image following the hybridization of Cy3-labeled complementary oligonucleotides onto DNA-Au NPs on SiO_2 patterned with EUV (scale bar 20 μm). (B) Large-area fluorescence scan of the substrate following the hybridization (scale bar 1 mm). Shown is the projection through the whole mask area. (C) SEM image following the immobilization of DNA-Au NPs on nanopatterns of 55 nm width and a pitch of 110 nm on SiO_2 (scale bar 200 nm). (D) Fluorescence image following the hybridization onto double EUV patterned substrates (scale bar 50 μm). Shown is the mirror image of the word "CNTEU" with one sequence and the word "EUV" with the other sequence.

complementary oligonucleotides on the first patterns are at low levels, suggesting the binding between the DNA-Au NPs and the surface of the substrate is not reversible. This type of hybridization at the wrong spot was observed only in a very small portion (<∼5% of the contour length) of the 100 nm wide lines and was probably caused by the binding of second conjugates to the defect sites on the first set of patterns. These defect sites may be related to the variations in the exposure of small line width patterns along tens of micrometers, implied by the absence of such sites in the large-area patterns (Figure 5D).

We hypothesize that generation of positively charged regions with electron beam lithography for the site-specific immobilization of DNA molecules can be extended to parallel lithography systems, as similar charging phenomenon has been reported for other ionizing radiation sources.[30] In order to test this hypothesis, we performed experiments with EUV lithography, which uses a light source in the wavelength of 13.4 nm. EUV lithography is capable of generating nanoscale patterns[46] and considered as one of the leading candidates for the future fabrication of semiconductor chips.[47] Immobilization of DNA-Au NPs was performed as described previously except the EUV interference lithography system[48−50] at University of Wisconsin−Madison was used instead of electron beam lithography. As can be seen in Figure 5A, hybridization of the Cy3-labeled complement showed clearly site-specific fluorescence from EUV-exposed areas. Figure 5B shows a large area fluorescence scan (Axon 4000B microarray scanner) of the EUV patterned SiO_2 following the hybridization, demonstrating patterning of DNA over square millimeter areas with the advantage of a parallel lithography system. The layout of the mask used for the EUV experiments consisted of grating patterns (rectangular areas) surrounded by micrometer scale marks (crosses and letters). The grating patterns consisted of series of lines with spacing equal to the width of the lines in the sub-100 nm range. Therefore hybridization onto individual lines could not be resolved with the fluorescence due to the diffraction limits in the optical microscopy, and instead fluorescence from the whole rectangular area of the grating could be observed (see the boxes in Figure 5B). SEM imaging (Figure 5C) reveals the specific attachment of DNA-Au NPs onto the nanopatterns; however, only quasi-single-particle-wide lines with some distortion in the center positions could be obtained. Patterning multiple DNA sequences with the charge-mediated localization of DNA-Au NPs using EUV lithography is shown in Figure 5D, with high contrast fluorescence

between the two different sequences following the hybridization. The site-specific placement of DNA-Au NPs onto EUV-exposed regions shows the generalizability of the presented approach to other ionizing radiation sources. Parallel lithographic systems with specifically designed masks/templates can lead to wafer scale fabrication of nanoscale DNA patterns and enable many applications.

Further optimization of the process can lead to wafer scale fabrication of sub-50 nm DNA patterns using EUV lithography. The imperfect alignment (Figure 5C) of DNA-Au NPs on nanopatterns generated with EUV lithography points to the need for the improvement in the process. The key is aerial image contrast between the exposed and unexposed regions. In the case of electron beam lithography, for example, this contrast is very high, and the exposure dose as a function of position across a patterned region resembles a step function (0% on the background and 100% on the pattern). This contrast is mitigated only at the nanometer length scale by the proximity effect where secondary electrons escape from the patterned areas into the unexposed areas. On the other hand, the aerial image contrast in EUV lithography depends on the characteristics of the mask and the tool. In the case of EUV interference lithography, the exposure dose as a function of position across a grating pattern resembles a sinusoidal function,[51] and therefore the unexposed regions are not completely dark (0%). The reduced aerial image contrast may lead to the generation of positive charges in the unexposed regions within the grating patterns and result in imperfect alignment of the particles along the lines. Fabrication of masks that result in exposures with improved aerial image contrast could improve placement of DNA-Au NPs on the nanoscale patterns prepared by EUV interference lithography. It is also important to note that the interference lithography system[48−50] used in the EUV experiments has been developed for scientific studies that require high-resolution (40−100 nm) periodic patterns. Commercial EUV systems[46] may be designed to fabricate patterns of higher aerial image contrast and are not limited to periodic arrays.

CONCLUSIONS

The new technique described here enables patterning of multiple DNA sequences with high resolution down to 15 nm with minimum nonspecific binding to background and high hybridization efficiency using advanced lithography infrastructure. Technologies developed for the semiconductor industry including alignment[44] of different exposures can be directly transferred to the technique. Demonstrating the approach with different radiation sources shows promise for extending the technique to parallel lithography systems for applications that require wafer scale patterning. The ability to pattern and register oligonucleotides of different sequences at the nanometer length scale can address some challenges in the site-specific placement of DNA nanostructures. The approach could also be applied to other biomolecules such as proteins with the appropriate design of substrates and molecules.

METHODS

Substrate Preparation and Lithographic Patterning. Two types of insulating layers were used for the generation of charge patterns on silicon substrates (N/Phos ⟨100⟩ 0−100 ohm-cm, Montco Silicon Technologies Inc.): spin-coated hydrogen silsesquioxane and vapor-deposited SiO_2. The 40 nm thick HSQ was spin-coated on oxygen plasma (PE 200 Benchtop Plasma System, Plasma Etch, Inc.) cleaned silicon substrates. The desired thickness of HSQ was obtained either by dilution from Fox-12 (Dow Corning) or by direct use of XR 1541 (Dow Corning). HSQ-coated substrates were baked for 1 min at 90 °C before patterning to ensure removal of the solvent. For the second type of substrates, 100 nm thick SiO_2 was deposited by plasma-enhanced chemical vapor deposition (PT 70, Plasma-Therm) in a clean-room environment on a silicon substrate. Electron beam lithography was performed on a LEO 1550-VP scanning electron microscope equipped with a J. C. Nabity pattern generation system. Patterns were written using 1 and 20 keV electron beam energy with beam currents of ∼13.5 and ∼32.4 pA, respectively. Extreme ultraviolet lithography was performed at the Synchrotron Radiation Center[48] at the University of Wisconsin−Madison.

Preparation and Deposition of DNA-Conjugated Au Nanoparticles (DNA-Au NPs). DNA-Au NPs were prepared according to the previously published protocol.[26] Briefly, to a 1 mL solution of Au NPs (15 nm in diameter, Ted Pella) was added 8 μL of 250 μM disulfide-modified oligonucleotides (Integrated DNA Technologies), and the solution was mixed on an orbital rotator for 18 h. Then 125 μL (added as 5 × 25 μL) each of 1 M sodium chloride and 0.1 M sodium phosphate buffer were added to the Au NP−oligonucleotide solution, and again the solution was placed on an orbital rotator for 24 h. Excess oligonucleotides in the solution were removed by repeated centrifugation (25 min at 15000 rcf), and DNA-Au NPs were suspended in 0.3 M sodium chloride/10 mM sodium phosphate buffer. The concentration of DNA-Au NPs was determined by measurement of the absorbance of 520 nm wavelength light in a UV/vis spectrophotometer (Nanodrop). DNA-Au NPs were centrifuged and resuspended in 0.3 M sodium chloride/10 mM sodium phosphate buffer before each use to ensure the removal of unbound oligonucleotides from the solution. A 50 μL volume of 1 nM DNA-Au NPs in 0.3 M sodium chloride/10 mM sodium phosphate buffer was spotted onto the electron beam patterned region at room temperature in a humidified environment for 1 h. Following the deposition of DNA-Au NPs, substrates were washed in 0.3 M sodium chloride buffer and water (Millipore MiliQ purification system), 1 min each, and then dried with N_2.

Hybridization of Fluorophore-Labeled Oligonucleotides and Fluorescence Imaging. Hybridization experiments were conducted in "stick-on" hybridization chambers (SA 200, Secure Seal, Grace Biolabs). Patterned substrates were first treated with a prehybridization

solution (0.1 mg/mL herring sperm DNA, 0.1 mg/mL acetylated bovine serum albumin in a 0.45 M sodium chloride buffer) for 15 min at 45 °C. The prehybridization solution was then replaced with a hybridization mixture (0.1 μM complementary oligonucleotide, 0.1 mg/mL herring sperm DNA, 0.1 mg/mL acetylated bovine serum albumin in a 0.45 M sodium chloride buffer). Substrates were then treated with the hybridization mixture for 2 h at 45 °C. Following the hybridization, substrates were washed in 0.45, 0.3, and 0.03 M sodium chloride buffer, respectively (1 min each) and Ar dried. Fluorescence microscopy images were taken with a Nikon Epi E800 Eclipse microscope equipped with Metamorph image processing software.

Acknowledgment. This paper is dedicated to the memory of our colleague, mentor, and friend Professor Franco Cerrina, who tragically passed away during the preparation of the manuscript. This work was supported by NSF through the University of Wisconsin Nanoscale Science and Engineering Center (NSEC) (Grant No. DMR-0832760) and Materials Research Science and Engineering Center (MRSEC) (Grant No. DMR-0520527). This work was based in part upon research conducted at the Synchrotron Radiation Center, University of Wisconsin–Madison, which is supported by the NSF under Award DMR-0537588.

Supporting Information Available: Details and additional SEM images of the particle counts; additional SEM images of the unpatterned regions and small line-width patterns. This material is available free of charge *via* the Internet at http://pubs.acs.org.

REFERENCES AND NOTES

1. Brown, P. O.; Botstein, D. Exploring the New World of the Genome with DNA Microarrays. *Nat. Genet.* **1999**, *21*, 33–37.
2. Wang, J.; From, D. N. A. Biosensors to Gene Chips. *Nucleic Acids Res.* **2000**, *28*, 3011–3016.
3. Lalander, C. H.; Zheng, Y.; Dhuey, S.; Cabrini, S.; Bach, U. DNA-Directed Self-Assembly of Gold Nanoparticles onto Nanopatterned Surfaces: Controlled Placement of Individual Nanoparticles into Regular Arrays. *ACS Nano* **2010**, *4*, 6153–6161.
4. Braun, E.; Eichen, Y.; Sivan, U.; Ben-Yoseph, G. DNA-Templated Assembly and Electrode Attachment of a Conducting Silver Wire. *Nature* **1998**, *391*, 775–778.
5. Seeman, N. C. DNA in a Material World. *Nature* **2003**, *421*, 427–431.
6. Rothemund, P. W. K. Folding DNA to Create Nanoscale Shapes and Patterns. *Nature* **2006**, *440*, 297–302.
7. Sharma, J.; Chhabra, R.; Andersen, C. S.; Gothelf, K. V.; Yan, H.; Liu, Y. Toward Reliable Gold Nanoparticle Patterning on Self-Assembled DNA Nanoscaffold. *J. Am. Chem. Soc.* **2008**, *130*, 7820–7821.
8. Rinker, S.; Ke, Y. G.; Liu, Y.; Chhabra, R.; Yan, H. Self-Assembled DNA Nanostructures for Distance-Dependent Multivalent Ligand-Protein Binding. *Nat. Nanotechnol.* **2008**, *3*, 418–422.
9. Maune, H. T.; Han, S. P.; Barish, R. D.; Bockrath, M.; Goddard, W. A.; Rothemund, P. W. K.; Winfree, E. Self-Assembly of Carbon Nanotubes into Two-Dimensional Geometries Using DNA Origami Templates. *Nat. Nanotechnol.* **2010**, *5*, 61–66.
10. Kershner, R. J.; Bozano, L. D.; Micheel, C. M.; Hung, A. M.; Fornof, A. R.; Cha, J. N.; Rettner, C. T.; Bersani, M.; Frommer, J.; Rothemund, P. W. K.; *et al.* Placement and Orientation of Individual DNA Shapes on Lithographically Patterned Surfaces. *Nat. Nanotechnol.* **2009**, *4*, 557–561.
11. Gerdon, A. E.; Oh, S. S.; Hsieh, K.; Ke, Y.; Yan, H.; Soh, H. T. Controlled Delivery of DNA Origami on Patterned Surfaces. *Small* **2009**, *5*, 1942–1946.
12. Ding, B. Q.; Wu, H.; Xu, W.; Zhao, Z. A.; Liu, Y.; Yu, H. B.; Yan, H. Interconnecting Gold Islands with DNA Origami Nanotubes. *Nano Lett.* **2010**, *10*, 5065–5069.
13. Pearson, A. C.; Pound, E.; Woolley, A. T.; Linford, M. R.; Harb, J. N.; Davis, R. C. Chemical Alignment of DNA Origami to Block Copolymer Patterned Arrays of 5 nm Gold Nanoparticles. *Nano Lett.* **2011**, *11*, 1981–1987.
14. Noh, H.; Hung, A. M.; Choi, C.; Lee, J. H.; Kim, J. Y.; Jin, S.; Cha, J. N. 50 nm DNA Nanoarrays Generated from Uniform Oligonucleotide Films. *ACS Nano* **2009**, *3*, 2376–2382.
15. Park, J. U.; Lee, J. H.; Paik, U.; Lu, Y.; Rogers, J. A. Nanoscale Patterns of Oligonucleotides Formed by Electrohydrodynamic Jet Printing with Applications in Biosensing and Nanomaterials Assembly. *Nano Lett.* **2008**, *8*, 4210–4216.
16. Yu, A. A.; Savas, T. A.; Taylor, G. S.; Guiseppe-Elie, A.; Smith, H. I.; Stellacci, F. Supramolecular Nanostamping: Using DNA as Movable Type. *Nano Lett.* **2005**, *5*, 1061–1064.
17. Demers, L. M.; Ginger, D. S.; Park, S. J.; Li, Z.; Chung, S. W.; Mirkin, C. A. Direct Patterning of Modified Oligonucleotides on Metals and Insulators by Dip-Pen Nanolithography. *Science* **2002**, *296*, 1836–1838.
18. Shim, W.; Braunschweig, A. B.; Liao, X.; Chai, J. N.; Lim, J. K.; Zheng, G. F.; Mirkin, C. A. Hard-Tip, Soft-Spring Lithography. *Nature* **2011**, *469*, 516–521.
19. Wong, I. Y.; Melosh, N. A. Directed Hybridization and Melting of DNA Linkers using Counterion-Screened Electric Fields. *Nano Lett.* **2009**, *9*, 3521–3526.
20. Zhang, G. J.; Tanii, T.; Funatsu, T.; Ohdomari, I. Patterning of DNA Nanostructures on Silicon Surface by Electron Beam Lithography of Self-Assembled Monolayer. *Chem. Commun.* **2004**, 786–787.
21. Negrete, O. D.; Onses, M. S.; Nealey, P. F.; Cerrina, F. In Situ Synthesis and Direct Immobilization of ssDNA on Electron Beam Patterned Hydrogen Silsesquioxane. *J. Vac. Sci. Technol. B* **2009**, *27*, 3082–3087.
22. Yong, Y. C.; Thong, J. T. L.; Phang, J. C. H. Determination of Secondary Electron Yield From Insulators Due to a Low-kV Electron Beam. *J. Appl. Phys.* **1998**, *84*, 4543–4548.
23. Joo, J.; Chow, B. Y.; Jacobson, J. M. Nanoscale Patterning on Insulating Substrates by Critical Energy Electron Beam Lithography. *Nano Lett.* **2006**, *6*, 2021–2025.
24. Bernstein, G. H.; Polchlopek, S. W.; Kamath, R.; Porod, W. Determination of Fixed Electron-Beam Induced Positive Oxide Charge. *Scanning* **1992**, *14*, 345–349.
25. Chi, P. Y.; Lin, H. Y.; Liu, C. H.; Chen, C. D. Generation of Nano-Scaled DNA Patterns Through Electron-Beam Induced Charge Trapping. *Nanotechnology* **2006**, *17*, 4854–4858.
26. Taton, T. A. Preparation of Gold Nanoparticle-DNA Conjugates. *Current Protocols in Nucleic Acid Chemistry*; Wiley: New York,2002; Chapter 12, Unit 12 2.
27. Lin, H. Y.; Tsai, L. C.; Chen, C. D. Assembly of Nanoparticle Patterns with Single-Particle Resolution Using DNA-Mediated Charge Trapping Technique: Method and Applications. *Adv. Funct. Mater.* **2007**, *17*, 3182–3186.
28. Smith, D. E.; Chu, S. Response of Flexible Polymers to a Sudden Elongational Flow. *Science* **1998**, *281*, 1335–1340.
29. Seiler, H. Secondary-Electron Emission in the Scanning Electron-Microscope. *J. Appl. Phys.* **1983**, *54*, R1–R18.
30. Ma, T. P.; Dressendorfer, P. V. *Ionizing Radiation Effects in MOS Devices and Circuits*; Wiley: New York, 1989.
31. Pathak, P. *Electron Energy Loss Processes in Polymeric Solids Application to Nano-Lithography*; University of Wisconsin–Madison: Madison, WI, 2009.
32. Choi, S.; Word, M. J.; Kumar, V.; Adesida, I. Comparative Study of Thermally Cured and Electron-Beam-Exposed Hydrogen Silsesquioxane Resists. *J. Vac. Sci. Technol. B* **2008**, *26*, 1654–1659.
33. Choi, S.; Yan, M.; Adesida, I. Fabrication of Triangular Nanochannels Using the Collapse of Hydrogen Silsesquioxane Resists. *Appl. Phys. Lett.* **2008**, *93*), 163113-1–3.
34. Beaumont, A.; Dubuc, C.; Beauvais, J.; Drouin, D. Direct-Write Electron Beam Lithography in Silicon Dioxide at Low Energy. *J. Vac. Sci. Technol. B* **2010**, *28*, 940–945.
35. Broers, A. N. Resolution Limits for Electron-Beam Lithography. *IBM J. Res. Dev.* **1988**, *32*, 502–513.
36. Miura, N.; Ishii, H.; Yamada, A.; Konagai, M. Application of Carbonaceous Material for Fabrication of Nano-Wires with a Scanning Electron Microscopy. *Jpn. J. Appl. Phys. 2* **1996**, *35*, L1089–L1091.
37. Sarveswaran, K.; Hu, W. C.; Huber, P. W.; Bernstein, G. H.; Lieberman, M. Deposition of DNA Rafts on Cationic SAMs on Silicon [100]. *Langmuir* **2006**, *22*, 11279–11283.

38. Hurst, S. J.; Lytton-Jean, A. K. R.; Mirkin, C. A. Maximizing DNA Loading on a Range of Gold Nanoparticle Sizes. *Anal. Chem.* **2006**, *78*, 8313–8318.
39. Pirrung, M. C. How To Make a DNA Chip. *Angew. Chem., Int. Ed.* **2002**, *41*), 1276–1289.
40. Herne, T. M.; Tarlov, M. J. Characterization of DNA Probes Immobilized on Gold Surfaces. *J. Am. Chem. Soc.* **1997**, *119*, 8916–8920.
41. Belosludtsev, Y.; Iverson, B.; Lemeshko, S.; Eggers, R.; Wiese, R.; Lee, S.; Powdrill, T.; Hogan, M. DNA Microarrays Based on Noncovalent Oligonucleotide Attachment and Hybridization in Two Dimensions. *Anal. Biochem.* **2001**, *292*, 250–256.
42. Yang, M. S.; McGovern, M. E.; Thompson, M. Genosensor Technology and the Detection of Interfacial Nucleic Acid Chemistry. *Anal. Chim. Acta* **1997**, *346*, 259–275.
43. Guo, Z.; Guilfoyle, R. A.; Thiel, A. J.; Wang, R. F.; Smith, L. M. Direct Fluorescence Analysis of Genetic Polymorphisms by Hybridization with Oligonucleotide Arrays on Glass Supports. *Nucleic Acids Res.* **1994**, *22*, 5456–5465.
44. Laidler, D.; D'have, P. L., K.; Cheng, S. Sources of Overlay Error in Double Patterning Integration Schemes. *P. Soc. Photo-opt. Ins.* **2008**, *6922*, 69221E1–11.
45. Hung, A. M.; Micheel, C. M.; Bozano, L. D.; Osterbur, L. W.; Wallraff, G. M.; Cha, J. N. Large-Area Spatially Ordered Arrays of Gold Nanoparticles Directed by Lithographically Confined DNA Origami. *Nat. Nanotechnol.* **2010**, *5*, 121–126.
46. Wua, B. Q.; Kumar, A. Extreme Ultraviolet Lithography: A Review. *J. Vac. Sci. Technol. B* **2007**, *25*, 1743–1761.
47. International Technology Roadmap for Semiconductors. http://www.itrs.net.
48. Wallace, J.; Cheng, Y. C.; Isoyan, A.; Leonard, Q.; Fisher, M.; Green, M.; Bisognano, J.; Nealey, P. F.; Cerrina, F. A Novel EUVExposure Station for Nanotechnology Studies. *Nucl. Instrum. Methods A* **2007**, *582*, 254–257.
49. Solak, H. H.; David, C.; Gobrecht, J.; Golovkina, V.; Cerrina, F.; Kim, S. O.; Nealey, P. F. Sub-50 nm Period Patterns with EUV Interference Lithography. *Microelectron. Eng.* **2003**, *67−68*, 56–62.
50. Solak, H. H.; He, D.; Li, W.; Singh-Gasson, S.; Cerrina, F.; Sohn, B. H.; Yang, X. M.; Nealey, P. F. Exposure of 38 nm Period Grating Patterns with Extreme Ultraviolet Interferometric Lithography. *Appl. Phys. Lett.* **1999**, *75*, 2328–2330.
51. Isoyan, A.; Wuest, A.; Wallace, J.; Jiang, F.; Cerrina, F. 4X Reduction Extreme Ultraviolet Interferometric Lithography. *Opt. Express* **2008**, *16*, 9106–9111.